LANGMUIR
Cite This: Langmuir 2018, 34, 1750−1759
Article
pubs.acs.org/Langmuir

Protein−Substrate Adhesion in Microcontact Printing Regulates Cell Behavior

Shuhuan Hu,*[,†] Ting-Hsuan Chen,[†,‡] Yanhua Zhao,[†] Zuankai Wang,[†,‡] and Raymond H. W. Lam*[,†,‡]

[†]Department of Mechanical and Biomedical Engineering, City University of Hong Kong, Hong Kong
[‡]City University of Hong Kong, Shenzhen Research Institute, Shenzhen, China

Supporting Information

ABSTRACT: Microcontact printing (μCP) is widely used to create patterns of biomolecules essential for studies of cell mechanics, migration, and tissue engineering. However, different types of μCPs may create micropatterns with varied protein−substrate adhesion, which may change cell behaviors and pose uncertainty in result interpretation. Here, we characterize two μCP methods for coating extracellular matrix (ECM) proteins (stamp-off and covalent bond) and demonstrate for the first time the important role of protein−substrate adhesion in determining cell behavior. We found that, as compared to cells with weaker traction force (e.g., endothelial cells), cells with strong traction force (e.g., vascular smooth muscle cells) may delaminate the ECM patterns, which reduced cell viability as a result. Importantly, such ECM delamination was observed on patterns by stamp-off but not on the patterns by covalent bonds. Further comparisons of the displacement of the ECM patterns between the normal VSMCs and the force-reduced VSMCs suggested that the cell traction force plays an essential role in this ECM delamination. Together, our results indicated that μCPs with insufficient adhesion may lead to ECM delamination and cause cell death, providing new insight for micropatterning in cell−biomaterial interaction on biointerfaces.

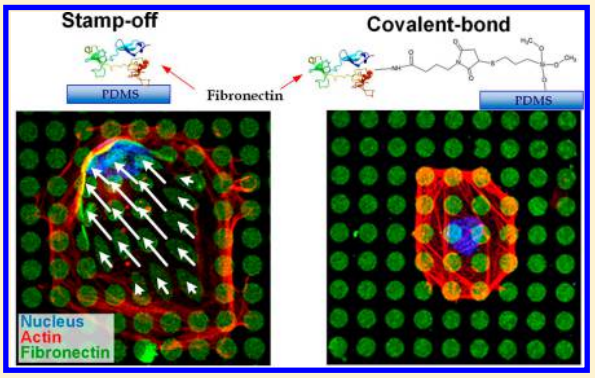

INTRODUCTION

Microcontact printing (μCP) is a widely used biofabrication method of coating or self-assembling macromolecules such as DNA, extracellular matrix (ECM) proteins, and antibodies with precisely defined micropatterns on planar substrates.[1−3] Over the past two decades, μCP has become a fundamental tool for cell research, drug screening, and tissue engineering.[4−7] In particular, μCP has enabled detailed studies on subcellular motility and the cytoskeleton mediated by well-defined adhesion sites confined by ECM proteins. For example, it has been reported that μCP can achieve collagen VI stripes with different spacing distances to regulate chondrocyte behavior for the development of cartilage replacement.[8] Recently, a new microcontact printing technique called pattern on topography (PoT) was developed to examine the synergistic regulating effects of biophysical and biochemical cues with respect to cardiomyocytes.[9]

The working principle of μCP mostly relies on cell adhesion to the ECM protein, which is essential for many physiological activities. At the cellular level, cell adhesion regulates apoptosis, mitogenesis, cell differentiation, and cell migration.[10−15] At the tissue/organ level, the adhesive property of ECM is required for tissue integrity[16−18] and was highlighted by many genetic and autoimmune diseases, such as muscular dystrophy.[19] Clinical practices have revealed the effectiveness of using immobilized ECM proteins in the central nervous system to repair nerves.[20] However, increasing evidence suggests that cells do not passively attach to ECM. Instead, this cell−ECM adhesion is a two-way mechanical interaction mediated by focal adhesions (FAs)[21−23] and cytoskeletal networks.[24−27] That is, the mechanical signals may transduce from ECM to cells and reorganize the cytoskeleton networks. As a result, the cellular force is then iteratively changed, causing a disruption of the constitution and structure of ECM.[28−31]

Early μCP methods involved the binding of molecules on a substrate through chemical reactions such as metal-alkanethiolate bonding,[32,33] silanization,[34] and carbodiimide cross-linking schemes.[33] More recently, researchers have implemented μCP using noncovalent bindings to achieve the more rapid and flexible micropatterns.[35,36] These μCP procedures usually include polymer surface activation, either oxygen plasma bombardment[2] or ultraviolet−ozone irradiation.[37] However, different μCP methods may create micropatterned ECM protein with varied protein−substrate adhesion. As a result, the cell traction force is resisted to different levels, leading to changes in cytoskeleton organization and regulation of cell behavior, but it is rarely addressed.

Received: August 19, 2017
Revised: November 30, 2017
Published: January 5, 2018

Downloaded via CITY UNIV OF HONG KONG on July 4, 2018 at 06:17:00 (UTC).
See https://pubs.acs.org/sharingguidelines for options on how to legitimately share published articles.

© 2018 American Chemical Society

DOI: 10.1021/acs.langmuir.7b02935
Langmuir 2018, 34, 1750−1759

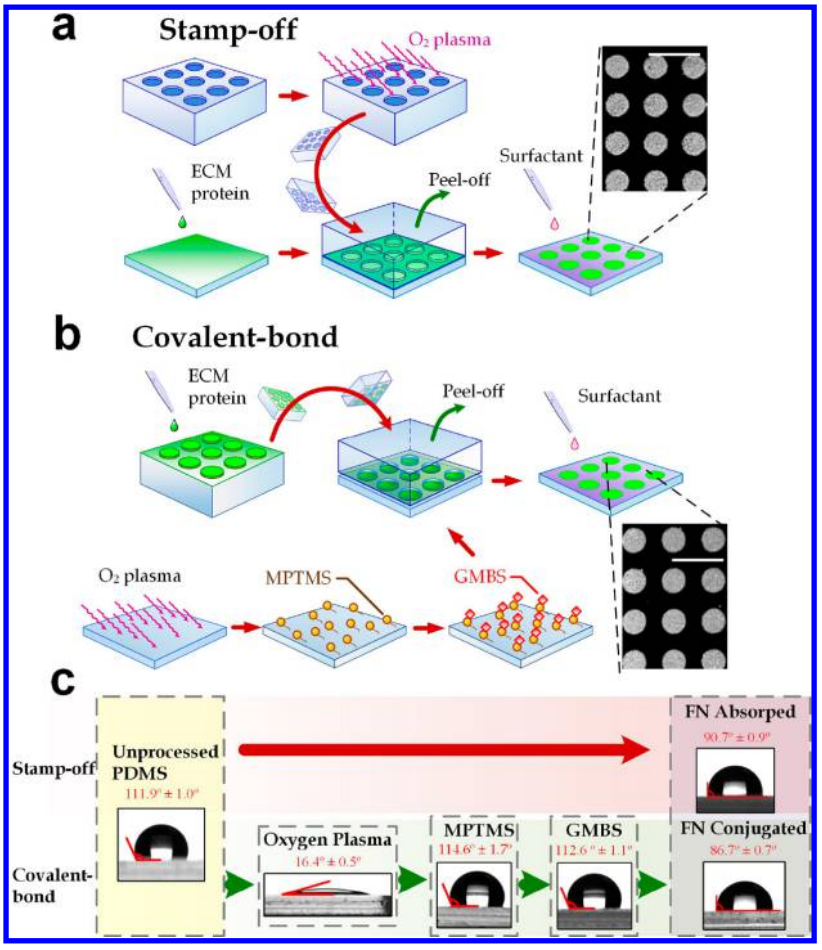

Figure 1. μCP of ECM proteins for achieving different protein−substrate adhesion using (a) stamp-off based on direct adsorption and (b) the covalent bond based on intermediate binding molecules. Scale bars in all insets: 10 μm. (c) Contact angles at different surface modification steps during the μCP processes. FN stands for fibronectin.

In this paper, we analyze cell behavior for growth on ECM protein micropatterns coated with two different μCP methods (stamp-off and covalent bond). The stamp-off patterning relies on the direct molecular adsorption while the covalent-bond scheme applies intermediating molecules with the higher binding strength by linking both ECM proteins and substrates with covalent bonds. We seed cells onto the substrates and inspect the role of protein−substrate adhesion in the two-way cell−ECM interactions. On the ECM side, we observe any changes in the protein patterns induced by the seeded cells. On the other side, we examine whether the cell characteristics such as morphology, viability, and cytoskeleton formation are different on the micropatterns coated with the different μCP methods.

EXPERIMENTAL SECTION

ECM Patterning Techniques. We adopted two μCP techniques (stamp-off and covalent bond) with different levels of protein−substrate adhesion. Poly(dimethylsiloxane) (PDMS), the widely used biocompatible polymeric material (Dow Corning, Midland, MI),[38] is used as the substrate. All of the PDMS substrates were cast from a trichloro(1*H*,1*H*,2*H*,2*H*-perfluorooctyl)silane (Sigma-Aldrich, St. Louis, MO)-treated flat silicon wafer with a monomer−curing agent in a weight ratio of 10:1 after baking at 80 °C for >20 h. In this work, we selected the fibronectin conjugated with fluorescent molecules (Alexa Fluor 488 protein label kit, Thermo Fisher Scientific, Waltham, MA) as the ECM protein for visualizing the coated protein patterns using the selected μCP methods.

The first μCP method (stamp-off) utilized a microstructured stamp to create patterns by removing ECM protein from some regions on a fibronectin-adsorbed PDMS substrate.[35] As shown in Figure 1a, we prepared a PDMS stamp (10:1 monomer−curing agent ratio) with microstructures of a negative pattern based on traditional soft lithography.[39] The PDMS stamp was prepared using the photolithography of SU-8 photoresist (Microchem) on a silicon wafer followed by the silanization of trichloro(1*H*,1*H*,2*H*,2H-perfluorooctyl)silane. The PDMS stamp was further treated with oxygen plasma (PDC001, Harrick Plasma, Ithaca, NY) to enhance its molecular adhesion to fibronectin. To coat fibronectin on the PDMS substrate, we pipetted 50 μg/mL fluorescent fibronectin in water to cover the PDMS substrate for 2 h in order to facilitate the protein adsorption. After blow-drying with compressed air, the microstructured PDMS stamp was placed on the flat fibronectin-coated PDMS for 20 s. As the plasma-treated PDMS stamp had a stronger molecular adhesion, fibronectin on the contact surfaces between the stamp and the substrate were removed after the stamp was peeled off.[35,40,41] We then applied a 0.1% surfactant (pluronic F127, Sigma-Aldrich) to the substrate for 15 min to prevent unexpected cell−substrate attachment in the uncoated regions and rinsed the substrate with distilled water.

The second μCP method (covalent bond) applied intermediate molecules to achieve covalent bonds between the protein coating and the substrate for stronger protein−substrate adhesion (Figure 1b). Ester-based protein immobilization was adapted to bind the fibronectin molecules onto the PDMS substrate through covalent bonding[42] (Figure 2a). Briefly, we treated the PDMS substrate with oxygen plasma, following by applying 4% (v/v) 3-mercaptopropyl trimethoxysilane (MPTMS; Gelest, Morrisville, PA) in ethanol to cover the PDMS substrate for 45 min. The substrate was washed with

DOI: 10.1021/acs.langmuir.7b02935
Langmuir 2018, 34, 1750−1759

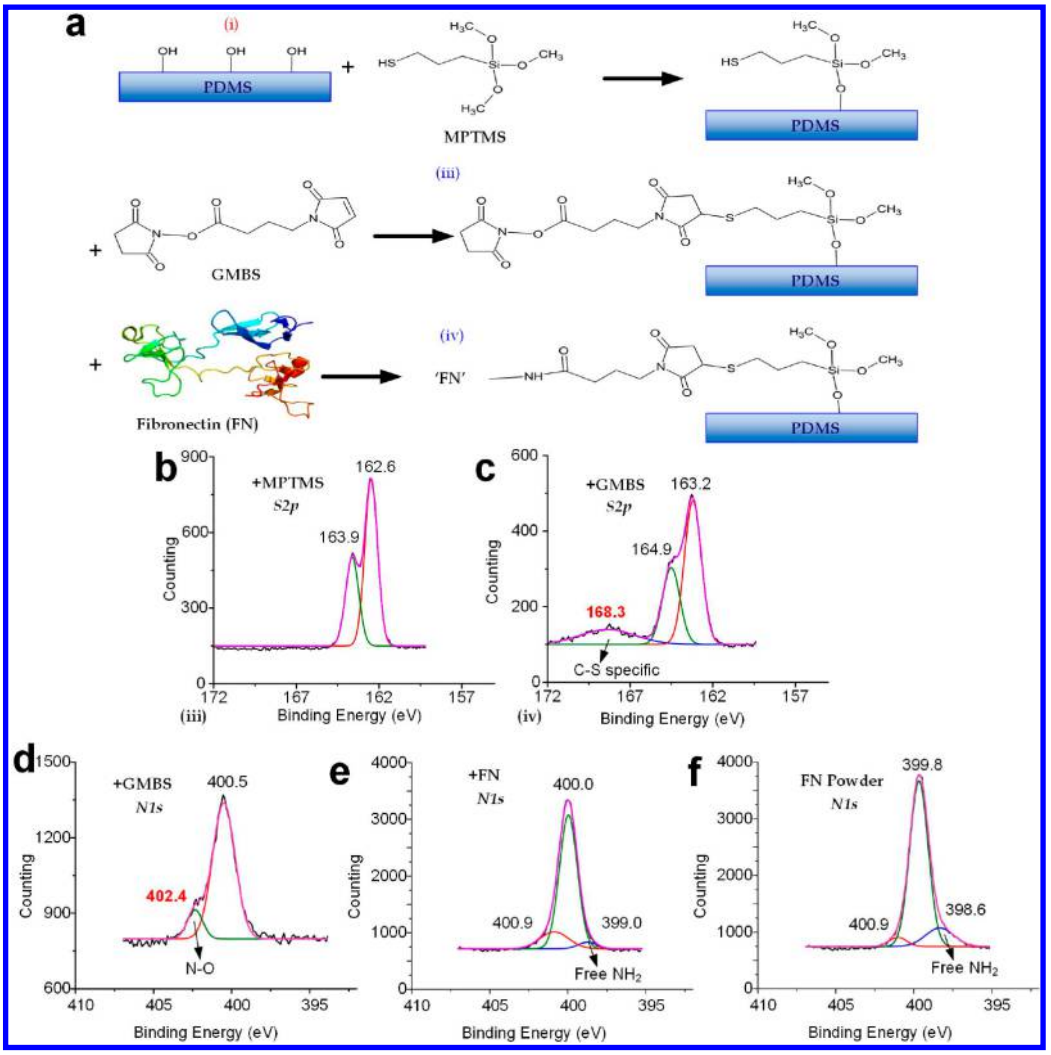

Figure 2. (a) Key chemical reactions at different steps in the ECM protein patterning based on covalently bonded molecules. (b–f) S 2p and N 1s XPS spectra at key steps in the covalent-bond method. All spectra were referenced to the C 1s peak of the PDMS substrate (284.8 eV). Deconvolutions were conducted to analyze the spectra.

ethanol and then covered with 0.28% (w/v) *N*-γ-maleimidobutyryloxy succinimide ester (GMBS, Thermo Fisher Scientific) in ethanol for another 15 min. On the other side, fibronectin was applied to a positive microstructured stamp. We then placed the stamp on the chemically treated substrate for 20 s. After the peeling of the stamp, we applied pluronic F127 and rinsed the substrate to avoid any unexpected cell attachment.

Surface Characterization. X-ray photoelectron spectroscopy (XPS) experiments were conducted using an XPS facility (PHI model 5802 with a monochromatic Al Kα X-ray source at 1486.6 eV; Physical Electronics, Chanhassen, MN) with a pressure of 10^{-10} mBar and a resolution of 0.1081 eV. Attenuated total reflectance Fourier transform infrared spectroscopy (ATR-FTIR, PerkinElmer 1600, PerkinElmer, Waltham, MA) together with a zinc selenide crystal was used to characterize the covalent bonds between molecules. An ellipsometer with a resolution of 0.1 nm (Jobin Yvon-PZ2000; Horiba Scientific, Edison, NJ) using a He–Ne laser (632.8 nm) was used to measure the thickness of the protein layer. The adhesion force was determined by the Universal Testing Machine (UTM-EZ-LX, Shimadzu Scientific Instruments, Columbia, MD). Immediately before the test, the moving plate (diameter: 8 mm) was treated with underwater glue (JH-5553; Jin Hong Glues, Hangzhou, China). The speed of the moving plate was set to 10 mm min^{-1} to obtain the load–displacement curve. The applied load was set as 10 N, and the contact time between the sample and the moving plate surface was 5 min. In addition, we measured the surface hydrophobicity and recorded infrared spectra of the fibronectin-coated substrates in different fabrication stages. The surface hydrophobicity was measured using a drop-shape analyzer (DSA100, Kruss, Hamburg, Germany).

Cell Culture. Primary human vascular smooth muscle cells (VSMCs; Lonza, Walkersville, MD) were cultured in the standard medium kit (SmGM-2 BulletKit, Lonza). Primary human umbilical vein endothelial cells (VECs; Lonza) were cultured in the standard medium kit (EGM-2 BulletKit, Lonza). NIH/3T3 fibroblasts (3T3; ATCC, Manassas, VA) were cultured in Dulbecco's modified Eagle's medium (DMEM; Life Technologies, Carlsbad, CA) supplemented with 10% bovine serum, 100 units/mL penicillin, and 1% L-glutamine. The cells were cultured in a 5% CO_2 humidified cell culture incubator at 37 °C. The cells were trypsinized and subcultured once their population reached >80% confluence. Only cells with a passage number <6 were used for the more consistent cell properties.

Cell Analysis. We performed cell viability tests using a live/dead viability/cytotoxicity kit (calcein AM for live cells and EthD-1 for dead cells; Thermo Fisher Scientific, Waltham, MA) such that the live and dead cells were stained with green and red fluorescent signals, respectively. In these tests, we used fibronectin without fluorescence in the μCP process to eliminate any disturbance to the GFP signals stained in live cells. To further investigate the correlation between FN disruption and cell viability, we seeded the cells on fluorescent 488-FN micropatterns, followed by staining the cells with 4 μM EthD-1 (from the live/dead assay kit) and 1 μg/mL Hoechst H33342 (Sigma-

DOI: 10.1021/acs.langmuir.7b02935
Langmuir 2018, 34, 1750–1759

Aldrich). Hoechst H33342 has been widely applied to live cell staining and does not cause cell death.[43]

The intracellular components (nucleus and cytoskeletal actin) were visualized by immunofluorescence staining on cells. The cells were fixed with 4% paraformaldehyde (PFA, Sigma-Aldrich) in phosphate-buffered saline (PBS, Sigma-Aldrich) for 10 min and then treated with 0.3% Triton X-100 in PBS for 10 min. We applied 10% goat serum for 1 h to avoid nonspecific binding of the staining molecules in the next steps. The cytoskeletal actin was stained with Alexa-555 conjugated phalloidin (Life Technologies) followed by staining the nucleus with 4′,6-diamidino-2-phenylindole (DAPI, Sigma-Aldrich) for 10 min.

For focal adhesion staining, cytoskeleton extraction was first conducted to remove the soluble vinculin proteins. The extraction buffer was prepared as a basal buffer (10 mM PIPES, 50 mM NaCl, 150 mM sucrose, 3 mM $MgCl_2$, and 0.5% Triton X-100; all chemicals were analytical grade, purchased from Sigma-Aldrich; pH was adjusted to 6.5−6.8) supplemented with 1 μg/mL aprotinin, 1 μg/mL leupeptin, and 1 μg/mL pepstatin (purchased from Sigma-Aldrich). The cells was rinsed with the chilled extraction buffer for 60 s. After being rinsed with chilled PBS, the sample was fixed with 4% PFA for 10 min. Then the cells were treated with 0.3% Triton X-100 (in PBS) for 10 min, flowing by blocking the cells with 10% goat serum for 1 h. The primary antibody (mouse monoclonal antivinculin primary antibody, Life Technologies) was added to the sample later for 1 h, following by adding secondary antibody (Alexa-647 conjugated goat-antimouse secondary antibody, Life Technologies) for another 1 h.

All fluorescence microscope images were taken on either a motorized inverted fluorescence microscope (TE300, Nikon, Melville, NY) or a laser scanning confocal microscope (TCS-SP8, Leica Microsystems, Wetzlar, Germany). The images were processed using ImageJ (NIH, Bethesda, MD).

Coherence of Actin Fiber Orientation. We have utilized a well-established algorithm[44] for microscopic images, followed by computing the coherence of the fiber orientation, Ψ_{actin}, with the equation

$$\psi_{actin} = \frac{\pi}{\pi - 2}\left\{\frac{\sum_{x,y} I(x, y)\cos[\theta(x, y) - \theta_{avg}]}{\sum_{x,y} I(x, y)} - \frac{2}{\pi}\right\} \quad (1)$$

where x and y are horizontal and vertical pixel locations in an image, respectively. $I(x, y)$ is the intensity of a image pixel; $\theta(x, y)$ is the fiber orientation angle at a pixel location; and θ_{avg} is the average orientation angle over the image. The angle $\theta(x, y) - \theta_{avg}$ is always adjusted to lie between −90 and 90°. Adjustment factors $2/\pi$ and $\pi/(\pi-2)$ ensure that $\Psi_{actin} = 0$ for random fiber orientations and $\Psi_{actin} = 1$ for strictly aligned actin fibers.

Circularity. To assess the polarization of the cell body and the focal adhesions, the circularity was obtained by circularity = $4\pi \times$ area/perimeter^2. Rounded shapes will give a higher circularity while polarized shapes will give a lower circularity.

Statistical Analysis. A two-tailed t-test was performed using commercial software (Excel, Microsoft, Seattle, WA). We considered a difference to be significant for $p < 0.05$.

RESULTS AND DISCUSSION

Surface Characterization. We first characterize the contact angles of surfaces by the selected μCP methods after key surface modification steps. The thickness of the coated protein layers was 36.5 ± 9.2 nm for stamp-off surfaces and 34.4 ± 11.8 nm for covalently bound surfaces. Here, we considered the fibronectin layers without any micropatterns for the contact angle measurements, achieved by skipping protein removal by the mold for the stamp-off process and using a flat mold without microstructures for the stamp-off and covalent-bond methods. As shown in Figure 1c, the initial PDMS surface exhibited a contact angle of 111.9 ± 1.0° before the μCP processes. For the stamp-off case, the contact angle decreased to 90.7 ± 0.9° after the fibronectin adsorption. For the covalent-bond method, the contact angle decreased to 16.4 ± 0.5° after the plasma treatment; the contact angles after conjugating MPTMS, GMBS, and fibronectin were 114.6 ± 1.7°, 112.6 ± 1.1°, and 86.7 ± 0.7°, respectively. The final contact angles of the two μCP methods are similar (90.7 versus 86.7°), which means that the wettability of the surfaces were well controlled between the two experimental groups.

We examined the chemical reaction processes in the covalent-bond method by XPS spectra (Figure 2b−f). There is a broad peak at 168.3 eV in the S 2p spectra after GMBS conjugation (Figure 2b,c). Previous reports pointed out that such a broad, high-binding energy peak is evidence of the formation of the chemical bond of C−S,[45,46] indicating the reaction between MPTMS and GMBS. Moreover, for the XPS spectra of N 1s, the disappearance of the peak at 402.4 eV (N−O bond[47]) indicates that the *N*-hydroxysuccinimide group is substituted and the FN is bonded to the substrate (Figure 2d,e). Furthermore, the ratio of the amino group (∼399.0 eV[48]) of the conjugated FN protein was significantly reduced, which also indicated the success of FN conjugation (Figure 2e,f). The surface chemical properties in the covalent-bond method were also characterized by ATR-FTIR for different samples: pure PDMS, after MPTMS treatment, and after GMBS treatment are shown in Figure S3. As noted, after treating the PDMS substrate with MPTMS, a C−C absorption (∼1270 and 1290 cm^{-1}) and an S−H absorption (∼2575 cm^{-1}) appear on the spectra, indicating the conjugation of MPTMS molecules on PDMS. After treating the PDMS surface with GMBS, the conjugation of GMBS molecules indicated by N−H absorption (∼3400 cm^{-1}) and C═O absorption (∼1735 cm^{-1}) could be observed in the spectra.

Delamination of ECM Protein Micropatterns. After patterning fluorescent fibronectin onto the substrates with different μCP methods, the pattern quality can be examined by the fluorescence intensity that represents the local density of fibronectin (insets in Figure 1). For demonstration, we extracted the intensity along a line on the patterns (Figure S1), of which a high contrast between the pattern (bright) and gap (dark) regions indicated good patterning fidelity. Moreover, the geometry of focal adhesions was strongly confined by the micropatterns fabricated by the stamp-off method as well as the covalent-bond method, which indicated the success of blocking the cell attachment from the unpatterned area by pluronic F127.

Cells, as living objects, often exert traction forces on the extracellular environment to which they attach. We chose a cell type with relatively large traction forces (i.e., the primary human vascular smooth muscle cells (VSMCs)) to examine any delamination of ECM patterns with the different μCP methods. VSMCs were seeded on substrates with uniform and micropatterned fibronectin layers, fabricated by the stamp-off and covalent-bond methods. For both the uniformly coated and micropatterned ECM protein substrates, the pattern delamination can be clearly observed on the stamp-off, but no pattern delamination was shown on the covalent-bond surfaces (Figure 3). Very likely, the ECM protein−substrate adhesion determines such a pattern delamination process. To give a brief validation, we measured the protein adhesion force by a mechanical test machine (see Experimental Section). The molecular binding strength by the stamp-off process is low (1.28 ± 0.34 kN/m^2) because the protein deposition is mainly based on the weak intermolecular forces.[49] In contrast, the chemical covalent-bond scheme obtains more than 8 times

DOI: 10.1021/acs.langmuir.7b02935
Langmuir 2018, 34, 1750−1759

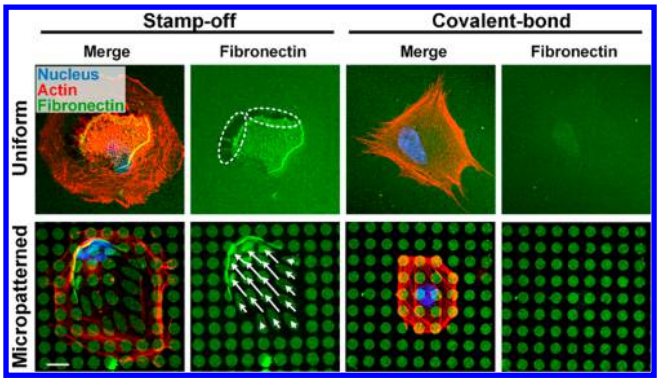

Figure 3. ECM protein delamination in cell spreading regions on uniform (upper) and micropatterned (lower) fibronectin layers. Hidden lines highlight the delamination regions of fibronectin. Arrows indicate displacements of the fibronectin microislands. Scale bar: 12 μm.

higher protein−substrate adhesion (11.9 ± 2.5 kN/m^2). (Figure S2) As a result, the traction force of cells was resisted.

Cell Traction Force in ECM Protein Delamination. A possible explanation of the ECM protein delamination is that a sufficiently large cell traction force may overcome the molecular binding and dislocate the protein patterns. To evaluate this possibility, we tested two other cell types with smaller cell traction forces than for VSMCs (6−10 kN/m^2):[50] 3T3 mouse fibroblasts (1.5 kN/m^2)[51] and human vascular endothelial cells (0.61 kN/m^2).[52] Our results show that 3T3 cells could induce pattern delamination only on the stamp-off surfaces but less often than that for VSMCs (Figure 4). The endothelial cells could not cause any pattern delamination (Figure 4). Thus, the occurrence frequency of pattern delamination seems to correlate with the cell types with different traction forces. In fact, these observations of pattern delamination matched well with the relative magnitude of the cell traction force in contrast to the protein−substrate adhesion forces: protein−substrate adhesion created by the stamp-off method (1.28 kN/m^2) could resist only the traction force exerted by VECs (0.61 kN/m^2) while the adhesion created by the covalent-bond method (11.9 kN/m^2) could resist the traction forces of all three cell types, even the VSMCs (6−10 kN/m^2) (Figure S2c).

To further validate the role of cell traction force, we have performed again the experiments with the blebbistatin-treated (50 μM) VSMCs growing on the μCP surfaces. In this case, the drug treatment would suppress the actomyosin traction force[53] and no pattern delamination was observed (Figure 5). Moreover, treating VSMCs with a small dosage of blebbistatin (50 μM in our case) significantly improved the viability of VSMCs on the stamp-off substrate (Figure S6), a phenomenon that has been reported earlier for culturing cardiac myocytes.[54] Thus, for a cell type with a larger traction force to disrupt the ECM protein, VSMC for example, protein−substrate adhesion can play a critical role in the cell−ECM interaction. Hence, selection of the correct μCP method for ECM protein patterns

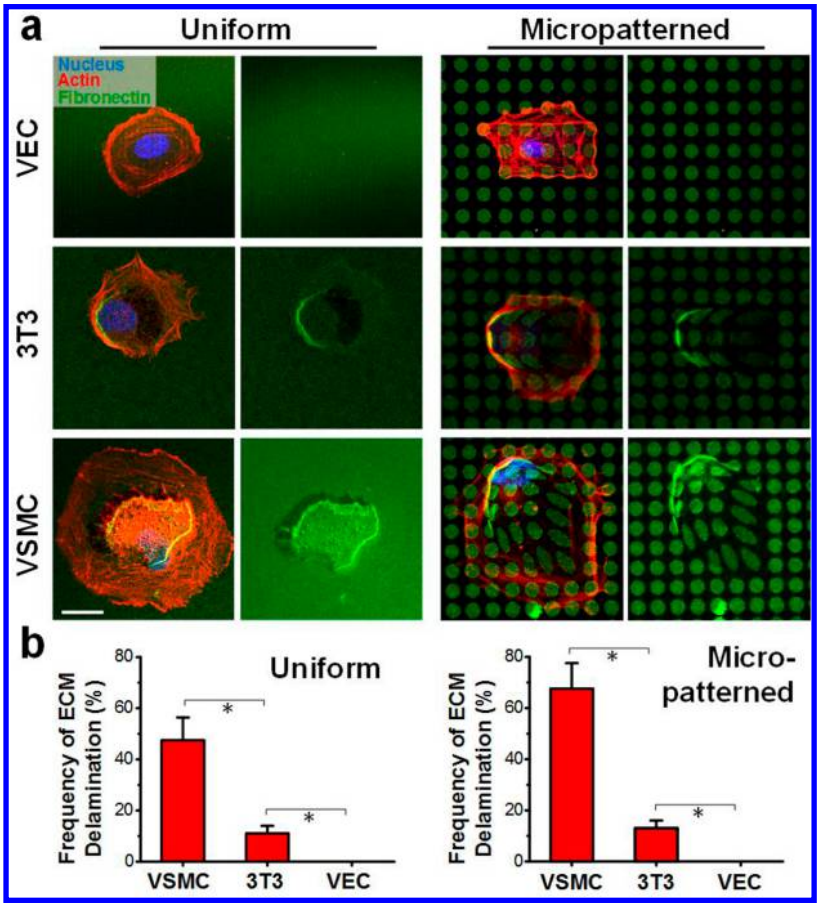

Figure 4. (a) VECs, 3T3 cells, and VSMCs on stamp-off surfaces with uniform and micropatterned fibronectin coatings. Scale bar: 25 μm. (b) Occurrence frequency of protein delamination of the different cell types on uniform and micropatterned surfaces. Note that the images for VSMCs are adapted from Figure 3.

DOI: 10.1021/acs.langmuir.7b02935
Langmuir 2018, 34, 1750−1759

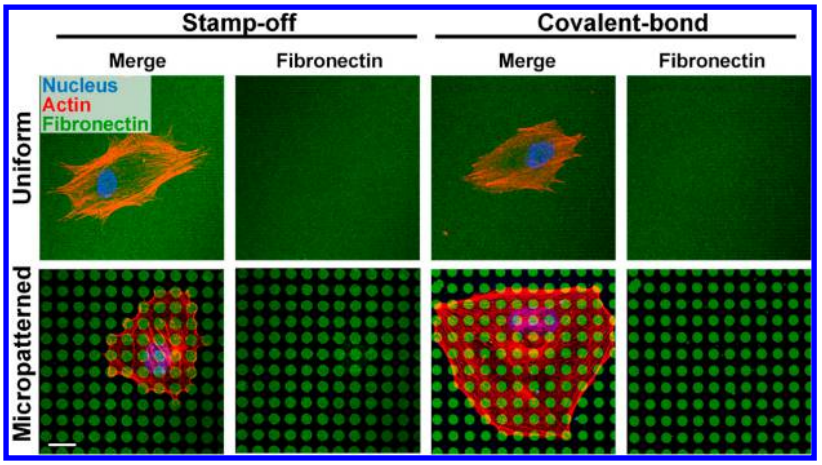

Figure 5. Micrographs of stained VSMCs treated with 50 μM blebbistatin (reducing the cell traction force by suppressing myosin II) on different μCP surfaces. Scale bar: 20 μm.

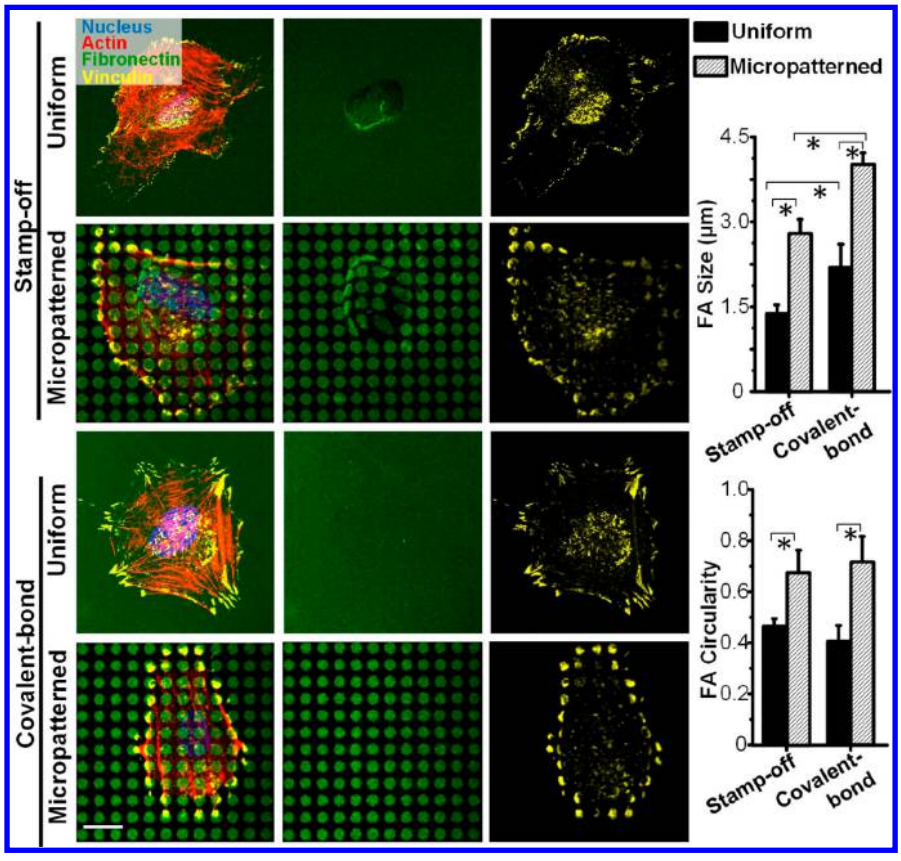

Figure 6. Focal adhesions (FA, represented by vinculin) of the VSMCs on micropatterned and uniform surfaces fabricated by different methods. Scale bar: 20 μm.

is particularly important for generating appropriate conditions for revealing relevant cell behaviors and promising cell analyses.

In fact, the interplay of ECM protein patterns and cellular traction force can be observed under many in vivo conditions, such as myofibroblasts and damaged ECM in the wound healing process,[55] vascular smooth muscle cells, and split ECM in the vascular repairing process.[56] Previous reports have also proposed the role of cellular mechanical stress in ECM deformation and stability,[24,57] especially in muscle fibers.[19] In these processes, it has been well studied that integrin plays an important role in the related cell migration and traction force modulation. For instance, the $\alpha5\beta1$ integrin binding to fibronectin is upregulated during the wound healing process.[55] Fibronectin displacement is considered to be a good indicator for integrin trafficking because of the many subtypes of integrin bind to fibronectin.[58] Similarly, the fibronectin dislocations toward the cell center as displayed in Figure 3 may indicate paths of integrin trafficking.[59]

Regulation of Cell Behaviors by Protein−Substrate Adhesion. Considering that the cell traction force can induce the delamination of the protein micropatterns with low protein−substrate adhesion, it is interesting to examine whether such binding strength is a biophysical factor affecting cell behavior as a two-way interaction. We further investigated

DOI: 10.1021/acs.langmuir.7b02935
Langmuir 2018, 34, 1750−1759

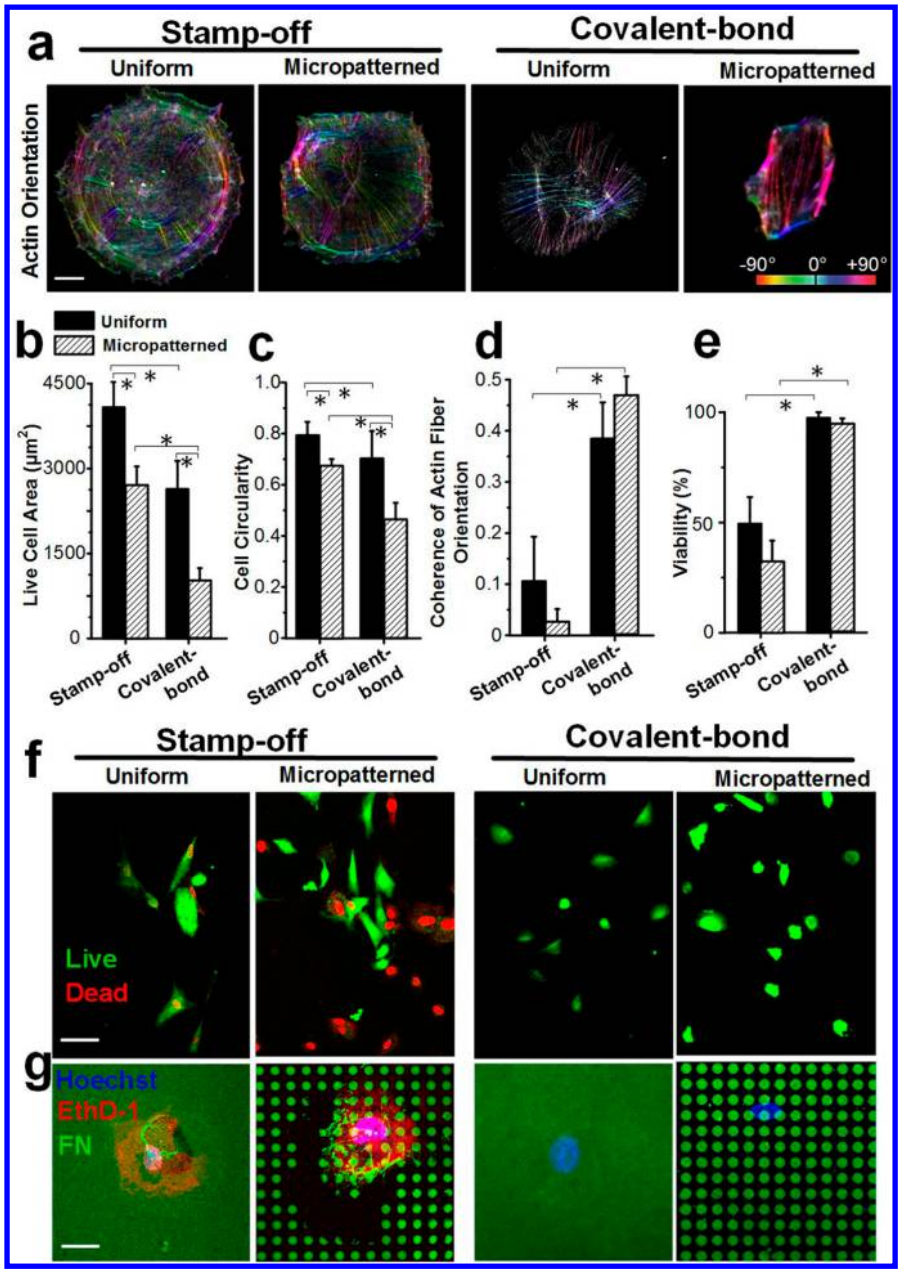

Figure 7. (a) Spatial maps of actin orientation. Scale bar: 10 μm. (b–e) Statistics of spreading areas, cell circularity, coherence of actin orientation, and viability of VSMCs on the μCP micropatterned fibronectin and on the uniform fibronectin. (f) Micrographs and statistics of the live (green) and dead (red) VSMCs cultured on the fibronectin micropatterns. Scale bar: 50 μm. (g) Correlations between FN delamination and VSMCs viability. Scale bar: 20 μm.

effects of the protein–substrate adhesion on the behavior of cells (e.g., focal adhesion formation, cell size, cell circularity, actin fiber orientation, and cell viability) growing on both uniform and micropatterned (Figures 6 and 7) fibronectin coatings.

An increase in focal adhesion size was found by comparing cells on micropatterns to those on uniform surfaces, and a further increase was observed with the use of the covalent-bond method (Figure 6). A previous report suggests a positive correlation between the size of the focal adhesion and the cell traction force.[60] As opposed to the highly polarized focal adhesions on the uniform surfaces, focal adhesions were strongly confined to a round shape when cultured on the micropatterns fabricated by either the stamp-off method or the covalent-bond method.[61,62] More importantly, the increased size of focal adhesions on micropatterns and covalent-bond surfaces implies a stronger traction force on such a substrate.[63] As a result, the increase in traction force, which was known to stimulate the formation of bundled stress fibers, may lead to a shrinkage in cell spreading[64] and a decrease in cell circularity[65] such that smaller and more anisotropic cells were observed on micropatterns and covalent-bond surfaces (Figure 7b,c).

It is important to note that such an increase in the traction force, accompanying by decreases in cell spreading and circularity, do not seem to be the reason for higher cell viability. For cells on a micropatterned surface, cells generally exhibited a greater FA size (Figure 6, which corresponds to a higher traction force) and decreased cell spreading and circularity (Figure 7b,c) than did cells on a uniform surface. Importantly, between cells on micropattered and uniform

DOI: 10.1021/acs.langmuir.7b02935
Langmuir 2018, 34, 1750–1759

surfaces, the difference in cell morphology did not cause a difference in cell viability (Figure 7e). Thus, it seems that cell live/dead is not simply brought about through the cell morphological change.[66]

On the other hand, higher cell viability and increased coherence of actin orientation were found only on the covalent-bond surface, indicating the importance of protein−substrate adhesion (Figure 7d). In general, ECM plays a role in stabilizing actin fibers by resisting the cellular force, and the rigorous disruption of ECM may induce cell apoptosis,[19] especially for those cell types with a higher traction force.[67] Thus, the increased protein−substrate adhesion is likely needed to stimulate and maintain the formation of bundled stress fibers, which is the hallmark of normal muscle cells,[68−70] and contributes to higher cell viability.[71] On the contrary, for a surface prepared by the stamp-off method, the weaker protein−substrate adhesion can result in protein delamination, which is equivalent to unstable or disrupted ECM and causes subcellular reorganization (actin fiber orientation and focal adhesion formation)[72] as well as lower cell viability. The correlation between cell viability and FN delamination was also proved by the coexistence of ECM disruption and cell death (Figures 7f,g and S5). Considering the lower viability caused by ECM delamination, stable ECM protein deposition is thus crucial to the long-term growth of cells, especially for those cell types with a higher traction force.[67]

Fabricating micropatterned surfaces to investigate cell−ECM interactions has led to many emerging findings in subcellular behavior, such as size-dependent smooth muscle actin recruitment during focal adhesion maturation,[73] asymmetric focal adhesion assembly,[62] and integrin subcellular segregation.[41] By considering the previously ignored cell mechanical feedback (i.e., ECM delamination by VSMCs) onto the extracellular environment,[62,74] we revealed that the feedback could again influence the cell behavior. Moreover, for the cell types with a smaller traction force (e.g., VECs and 3T3 fibroblasts in Figure S4), the differences in some cell behaviors (cell size and circularity) on the stamp-off surface and covalent-bond surface diminished. While this phenomenon could not be generalized to all cell types, our results provide an important demonstration that for the cell type with a large cell traction force such as VMSCs and possibly other cell types with a large traction force (myofibroblasts, cardiac smooth muscle cells, etc.), mechanical feedback may delaminate the ECM protein in micropatterning, which may lead to uncertainty in the interpretation of results and should not be ignored.

CONCLUSIONS

In this research, we adopted two microcontact printing (μCP) techniques (stamp-off and covalent-bond) to reveal for the first time the role of ECM protein−substrate adhesion in cell growth as a cell−ECM interaction. We observed that the delamination of the ECM protein micropatterns can be affected by both the protein−substrate adhesion and the cell traction force. We further demonstrated that protein−substrate adhesion can determine important cell characteristics such as cell viability and subcellular cytoskeletal arrangements.

Altogether, though μCP methods can generate micropatterned ECM protein layers with equivalent biochemical properties, the selection of the μCP methods is a critical concern in offering proper protein−substrate adhesion in the representative biophysical environments for cell and tissue applications. These results can offer important insights into the cell−ECM interactions as well as the surface-functionalized biomaterials and tissue engineering applications.

ASSOCIATED CONTENT

Supporting Information

The Supporting Information is available free of charge on the ACS Publications website at DOI: 10.1021/acs.langmuir.7b02935.

Adhesion force between the ECM protein and the substrates; ATR-FTIR spectra at the key micropatterning steps; mophorlogy of VECs and 3T3 cells on the micropatterned substrates; correlations between the ECM protein delamination and the cell death; and viability of blebbistatin-treated VSMCs on the micropatterned substrates. (PDF)

AUTHOR INFORMATION

Corresponding Authors

*E-mail: shuhuanhu2-c@my.cityu.edu.hk. Tel: +852-3442-7174.

*E-mail: rhwlam@cityu.edu.hk. Tel: +852-3442-8577. Fax: +852-3442-0172.

ORCID

Shuhuan Hu: 0000-0002-4163-1242

Zuankai Wang: 0000-0002-3510-1122

Raymond H. W. Lam: 0000-0002-5188-3830

Notes

The authors declare no competing financial interest.

ACKNOWLEDGMENTS

We acknowledge financial support from the National Natural Science Foundation of China (project no. 31500758), a General Research Grant (project no. 11206014), the Collaborative Research Fund (project no. C1013-15GF) of the Hong Kong Research Grant Council, the Croucher Foundation (startup grant), and the City University of Hong Kong (project no. 7004602).

REFERENCES

(1) Bernard, A.; Renault, J. P.; Michel, B.; Bosshard, H. R.; Delamarche, E. Microcontact printing of proteins. *Adv. Mater.* **2000**, *12* (14), 1067−1070.

(2) Schmalenberg, K.; Buettner, H.; Uhrich, K. Microcontact printing of proteins on oxygen plasma-activated poly (methyl methacrylate). *Biomaterials* **2004**, *25* (10), 1851−1857.

(3) Wang, Z.; Zhang, P.; Kirkland, B.; Liu, Y.; Guan, J. Microcontact printing of polyelectrolytes on PEG using an unmodified PDMS stamp for micropatterning nanoparticles, DNA, proteins and cells. *Soft Matter* **2012**, *8* (29), 7630−7637.

(4) Huebsch, N.; Arany, P. R.; Mao, A. S.; Shvartsman, D.; Ali, O. A.; Bencherif, S. A.; Rivera-Feliciano, J.; Mooney, D. J. Harnessing traction-mediated manipulation of the cell/matrix interface to control stem-cell fate. *Nat. Mater.* **2010**, *9* (6), 518−526.

(5) Cavalcanti-Adam, E. A.; Volberg, T.; Micoulet, A.; Kessler, H.; Geiger, B.; Spatz, J. P. Cell spreading and focal adhesion dynamics are regulated by spacing of integrin ligands. *Biophys. J.* **2007**, *92* (8), 2964−2974.

(6) Perl, A.; Reinhoudt, D. N.; Huskens, J. Microcontact printing: limitations and achievements. *Adv. Mater.* **2009**, *21* (22), 2257−2268.

(7) Hamon, C.; Henriksen-Lacey, M.; La Porta, A.; Rosique, M.; Langer, J.; Scarabelli, L.; Montes, A. B. S.; González-Rubio, G.; de Pancorbo, M. M.; Liz-Marzán, L. M. Tunable Nanoparticle and Cell

Assembly Using Combined Self-Powered Microfluidics and Microcontact Printing. *Adv. Funct. Mater.* **2016**, *26* (44), 8053−8061.
(8) Pan, C.-J.; Ding, H.-Y.; Dong, Y.-X. Extracellular matrix protein patterns guide human chondrocytes adhesion and alignment characterized by vimentin and matrilin-3. *Colloids Surf., B* **2013**, *102*, 730−736.
(9) Sun, Y.; Jallerat, Q.; Szymanski, J. M.; Feinberg, A. W. Conformal nanopatterning of extracellular matrix proteins onto topographically complex surfaces. *Nat. Methods* **2015**, *12* (2), 134−136.
(10) Dedhar, S. Cell−substrate interactions and signaling through ILK. *Curr. Opin. Cell Biol.* **2000**, *12* (2), 250−256.
(11) Bourgine, P. E.; Scotti, C.; Pigeot, S.; Tchang, L. A.; Todorov, A.; Martin, I. Osteoinductivity of engineered cartilaginous templates devitalized by inducible apoptosis. *Proc. Natl. Acad. Sci. U. S. A.* **2014**, *111* (49), 17426−17431.
(12) Sobers, C. J.; Wood, S. E.; Mrksich, M. A gene expression-based comparison of cell adhesion to extracellular matrix and RGD-terminated monolayers. *Biomaterials* **2015**, *52*, 385−394.
(13) Mui, K. L.; Bae, Y. H.; Gao, L.; Liu, S.-L.; Xu, T.; Radice, G. L.; Chen, C. S.; Assoian, R. K. N-cadherin induction by ECM stiffness and FAK overrides the spreading requirement for proliferation of vascular smooth muscle cells. *Cell Rep.* **2015**, *10* (9), 1477−1486.
(14) Gautrot, J. E.; Malmström, J.; Sundh, M.; Margadant, C.; Sonnenberg, A.; Sutherland, D. S. The nanoscale geometrical maturation of focal adhesions controls stem cell differentiation and mechanotransduction. *Nano Lett.* **2014**, *14* (7), 3945−3952.
(15) de Oliveira Ramos, G.; Bernardi, L.; Lauxen, I.; Sant'Ana Filho, M.; Horwitz, A. R.; Lamers, M. L. Fibronectin modulates cell adhesion and signaling to promote single cell migration of highly invasive oral squamous cell carcinoma. *PLoS One* **2016**, *11* (3), e0151338.
(16) Gumbiner, B. M. Cell Adhesion: The Molecular Basis of Tissue Architecture and Morphogenesis. *Cell* **1996**, *84* (3), 345−357.
(17) Sivakumar, P.; Czirok, A.; Rongish, B. J.; Divakara, V. P.; Wang, Y.-P.; Dallas, S. L. New insights into extracellular matrix assembly and reorganization from dynamic imaging of extracellular matrix proteins in living osteoblasts. *J. Cell Sci.* **2006**, *119* (7), 1350−1360.
(18) Dutta, R. C.; Dutta, A. K. Comprehension of ECM-Cell dynamics: A prerequisite for tissue regeneration. *Biotechnol. Adv.* **2010**, *28* (6), 764−769.
(19) Campbell, K. P. Three muscular dystrophies: loss of cytoskeleton-extracellular matrix linkage. *Cell* **1995**, *80* (5), 675−679.
(20) Zhang, Z.; Yoo, R.; Wells, M.; Beebe, T. P., Jr; Biran, R.; Tresco, P. Neurite outgrowth on well-characterized surfaces: preparation and characterization of chemically and spatially controlled fibronectin and RGD substrates with good bioactivity. *Biomaterials* **2005**, *26* (1), 47−61.
(21) Geiger, B.; Bershadsky, A.; Pankov, R.; Yamada, K. M. Transmembrane crosstalk between the extracellular matrix and the cytoskeleton. *Nat. Rev. Mol. Cell Biol.* **2001**, *2* (11), 793−805.
(22) Mooney, D. J.; Langer, R.; Ingber, D. E. Cytoskeletal filament assembly and the control of cell spreading and function by extracellular matrix. *Journal of Cell Science* **1995**, *108* (6), 2311−2320.
(23) Chen, C. S.; Tan, J.; Tien, J. Mechanotransduction at cell-matrix and cell-cell contacts. *Annu. Rev. Biomed. Eng.* **2004**, *6*, 275−302.
(24) Wang, N.; Butler, J. P.; Ingber, D. E. Mechanotransduction across the cell surface and through the cytoskeleton. *Science* **1993**, *260* (5111), 1124−1127.
(25) Katsumi, A.; Orr, A. W.; Tzima, E.; Schwartz, M. A. Integrins in mechanotransduction. *J. Biol. Chem.* **2004**, *279* (13), 12001−12004.
(26) Wang, N.; Tytell, J. D.; Ingber, D. E. Mechanotransduction at a distance: mechanically coupling the extracellular matrix with the nucleus. *Nat. Rev. Mol. Cell Biol.* **2009**, *10* (1), 75−82.
(27) Dupont, S.; Morsut, L.; Aragona, M.; Enzo, E.; Giulitti, S.; Cordenonsi, M.; Zanconato, F.; Le Digabel, J.; Forcato, M.; Bicciato, S. Role of YAP/TAZ in mechanotransduction. *Nature* **2011**, *474* (7350), 179−183.
(28) Guilak, F.; Cohen, D. M.; Estes, B. T.; Gimble, J. M.; Liedtke, W.; Chen, C. S. Control of stem cell fate by physical interactions with the extracellular matrix. *Cell Stem Cell* **2009**, *5* (1), 17−26.
(29) Streuli, C. Extracellular matrix remodelling and cellular differentiation. *Curr. Opin. Cell Biol.* **1999**, *11* (5), 634−640.
(30) Yoon, J.; Kim, J.; Jeong, H. E.; Sudo, R.; Park, M.-J.; Chung, S. Fabrication of type I collagen microcarrier using a microfluidic 3D T-junction device and its application for the quantitative analysis of cell−ECM interactions. *Biofabrication* **2016**, *8* (3), 035014.
(31) Swaminathan, V.; Waterman, C. M. The molecular clutch model for mechanotransduction evolves. *Nat. Cell Biol.* **2016**, *18* (5), 459−461.
(32) Wilbur, J. L.; Kumar, A.; Kim, E.; Whitesides, G. M. Microfabrication by microcontact printing of self-assembled monolayers. *Adv. Mater.* **1994**, *6* (7−8), 600−604.
(33) Lahiri, J.; Ostuni, E.; Whitesides, G. M. Patterning ligands on reactive SAMs by microcontact printing. *Langmuir* **1999**, *15* (6), 2055−2060.
(34) Delamarche, E.; Donzel, C.; Kamounah, F. S.; Wolf, H.; Geissler, M.; Stutz, R.; Schmidt-Winkel, P.; Michel, B.; Mathieu, H. J.; Schaumburg, K. Microcontact printing using poly (dimethylsiloxane) stamps hydrophilized by poly (ethylene oxide) silanes. *Langmuir* **2003**, *19* (21), 8749−8758.
(35) Weng, S.; Fu, J. Synergistic regulation of cell function by matrix rigidity and adhesive pattern. *Biomaterials* **2011**, *32* (36), 9584−9593.
(36) Xia, J.; Wang, Z.; Huang, D.; Yan, Y.; Li, Y.; Guan, J. Asymmetric biodegradable microdevices for cell-borne drug delivery. *ACS Appl. Mater. Interfaces* **2015**, *7* (11), 6293−6299.
(37) Wu, M. H. Simple poly (dimethylsiloxane) surface modification to control cell adhesion. *Surf. Interface Anal.* **2009**, *41* (1), 11−16.
(38) Bélanger, M. C.; Marois, Y. Hemocompatibility, biocompatibility, inflammatory and in vivo studies of primary reference materials low-density polyethylene and polydimethylsiloxane: A review. *J. Biomed. Mater. Res.* **2001**, *58* (5), 467−477.
(39) Xia, Y.; Whitesides, G. M. Soft lithography. *Annu. Rev. Mater. Sci.* **1998**, *28* (1), 153−184.
(40) Cavallini, M.; Gentili, D.; Greco, P.; Valle, F.; Biscarini, F. Micro-and nanopatterning by lithographically controlled wetting. *Nat. Protoc.* **2012**, *7* (9), 1668−1676.
(41) Desai, R. A.; Khan, M. K.; Gopal, S. B.; Chen, C. S. Subcellular spatial segregation of integrin subtypes by patterned multicomponent surfaces. *Integrative Biology* **2011**, *3* (5), 560−567.
(42) Stott, S. L.; Hsu, C.-H.; Tsukrov, D. I.; Yu, M.; Miyamoto, D. T.; Waltman, B. A.; Rothenberg, S. M.; Shah, A. M.; Smas, M. E.; Korir, G. K. Isolation of circulating tumor cells using a microvortex-generating herringbone-chip. *Proc. Natl. Acad. Sci. U. S. A.* **2010**, *107* (43), 18392−18397.
(43) Schmid, I.; Uittenbogaart, C.; Jamieson, B. D. Live-cell assay for detection of apoptosis by dual-laser flow cytometry using Hoechst 33342 and 7-amino-actinomycin D. *Nat. Protoc.* **2007**, *2* (1), 187−190.
(44) Forster, B.; Van De Ville, D.; Berent, J.; Sage, D.; Unser, M. Complex wavelets for extended depth-of-field: A new method for the fusion of multichannel microscopy images. *Microsc. Res. Tech.* **2004**, *65* (1−2), 33−42.
(45) Zheng, S.; Han, P.; Han, Z.; Zhang, H.; Tang, Z.; Yang, J. High performance C/S composite cathodes with conventional carbonate-based electrolytes in Li-S battery. *Sci. Rep.* **2015**, *4*,10.1038/srep04842.
(46) Yang, Y.; Yu, G.; Cha, J. J.; Wu, H.; Vosgueritchian, M.; Yao, Y.; Bao, Z.; Cui, Y. Improving the performance of lithium−sulfur batteries by conductive polymer coating. *ACS Nano* **2011**, *5* (11), 9187−9193.
(47) Zhao, M.; Cao, Y.; Liu, X.; Deng, J.; Li, D.; Gu, H. Effect of nitrogen atomic percentage on N+-bombarded MWCNTs in cytocompatibility and hemocompatibility. *Nanoscale Res. Lett.* **2014**, *9* (1), 142.
(48) Das, S.; Banquy, X.; Zappone, B.; Greene, G. W.; Jay, G. D.; Israelachvili, J. N. Synergistic interactions between grafted hyaluronic acid and lubricin provide enhanced wear protection and lubrication. *Biomacromolecules* **2013**, *14* (5), 1669−1677.
(49) Sibarani, J.; Takai, M.; Ishihara, K. Surface modification on microfluidic devices with 2-methacryloyloxyethyl phosphorylcholine polymers for reducing unfavorable protein adsorption. *Colloids Surf., B* **2007**, *54* (1), 88−93.

DOI: 10.1021/acs.langmuir.7b02935
Langmuir 2018, 34, 1750−1759

(50) Balasubramanian, L.; Lo, C.-M.; Sham, J. S.; Yip, K.-P. Remanent cell traction force in renal vascular smooth muscle cells induced by integrin-mediated mechanotransduction. *American Journal of Physiology-Cell Physiology* **2013**, *304* (4), C382−C391.
(51) Oakes, P. W.; Banerjee, S.; Marchetti, M. C.; Gardel, M. L. Geometry regulates traction stresses in adherent cells. *Biophys. J.* **2014**, *107* (4), 825−833.
(52) Kolodney, M. S.; Wysolmerski, R. B. Isometric contraction by fibroblasts and endothelial cells in tissue culture: a quantitative study. *J. Cell Biol.* **1992**, *117* (1), 73−82.
(53) Kovács, M.; Tóth, J.; Hetényi, C.; Málnási-Csizmadia, A.; Sellers, J. R. Mechanism of blebbistatin inhibition of myosin II. *J. Biol. Chem.* **2004**, *279* (34), 35557−35563.
(54) Kabaeva, Z.; Zhao, M.; Michele, D. E. Blebbistatin extends culture life of adult mouse cardiac myocytes and allows efficient and stable transgene expression. *American Journal of Physiology-Heart and Circulatory Physiology* **2008**, *294* (4), H1667−H1674.
(55) Huveneers, S.; Danen, E. H. Adhesion signaling−crosstalk between integrins, Src and Rho. *J. Cell Sci.* **2009**, *122* (8), 1059−1069.
(56) Majesky, M. W.; Dong, X. R.; Regan, J. N.; Hoglund, V. J. Vascular smooth muscle progenitor cells building and repairing blood vessels. *Circ. Res.* **2011**, *108* (3), 365−377.
(57) Petroll, W. M.; Ma, L.; Jester, J. V. Direct correlation of collagen matrix deformation with focal adhesion dynamics in living corneal fibroblasts. *J. Cell Sci.* **2003**, *116* (8), 1481−1491.
(58) Miyamoto, S.; Teramoto, H.; Coso, O. A.; Gutkind, J. S.; Burbelo, P. D.; Akiyama, S. K.; Yamada, K. M. Integrin function: molecular hierarchies of cytoskeletal and signaling molecules. *J. Cell Biol.* **1995**, *131* (3), 791−805.
(59) Bridgewater, R. E.; Norman, J. C.; Caswell, P. T. Integrin trafficking at a glance. *J. Cell Sci.* **2012**, *125* (16), 3695−3701.
(60) Tan, J. L.; Tien, J.; Pirone, D. M.; Gray, D. S.; Bhadriraju, K.; Chen, C. S. Cells lying on a bed of microneedles: an approach to isolate mechanical force. *Proc. Natl. Acad. Sci. U. S. A.* **2003**, *100* (4), 1484−1489.
(61) Balaban, N. Q.; Schwarz, U. S.; Riveline, D.; Goichberg, P.; Tzur, G.; Sabanay, I.; Mahalu, D.; Safran, S.; Bershadsky, A.; Addadi, L. Force and focal adhesion assembly: a close relationship studied using elastic micropatterned substrates. *Nat. Cell Biol.* **2001**, *3* (5), 466.
(62) Chen, C. S.; Alonso, J. L.; Ostuni, E.; Whitesides, G. M.; Ingber, D. E. Cell shape provides global control of focal adhesion assembly. *Biochem. Biophys. Res. Commun.* **2003**, *307* (2), 355−361.
(63) Liotta, L. A.; Kohn, E. C. The microenvironment of the tumour−host interface. *Nature* **2001**, *411* (6835), 375−379.
(64) Han, S. J.; Bielawski, K. S.; Ting, L. H.; Rodriguez, M. L.; Sniadecki, N. J. Decoupling Substrate Stiffness, Spread Area, and Micropost Density: A Close Spatial Relationship between Traction Forces and Focal Adhesions. *Biophys. J.* **2012**, *103* (4), 640−648.
(65) Wang, D.; Zheng, W.; Xie, Y.; Gong, P.; Zhao, F.; Yuan, B.; Ma, W.; Cui, Y.; Liu, W.; Sun, Y., Tissue-specific mechanical and geometrical control of cell viability and actin cytoskeleton alignment. *Sci. Rep.* **2015**, *4*, 10.1038/srep06160.
(66) Chen, C. S.; Mrksich, M.; Huang, S.; Whitesides, G. M.; Ingber, D. E. Geometric control of cell life and death. *Science* **1997**, *276* (5317), 1425−1428.
(67) Hald, E. S.; Steucke, K. E.; Reeves, J. A.; Win, Z.; Alford, P. W. Long-term vascular contractility assay using genipin-modified muscular thin films. *Biofabrication* **2014**, *6* (4), 045005.
(68) Lombardi, M. L.; Knecht, D. A.; Dembo, M.; Lee, J. Traction force microscopy in Dictyostelium reveals distinct roles for myosin II motor and actin-crosslinking activity in polarized cell movement. *J. Cell Sci.* **2007**, *120* (9), 1624−1634.
(69) Peyton, S. R.; Putnam, A. J. Extracellular matrix rigidity governs smooth muscle cell motility in a biphasic fashion. *J. Cell. Physiol.* **2005**, *204* (1), 198−209.
(70) Kumar, S.; Maxwell, I. Z.; Heisterkamp, A.; Polte, T. R.; Lele, T. P.; Salanga, M.; Mazur, E.; Ingber, D. E. Viscoelastic retraction of single living stress fibers and its impact on cell shape, cytoskeletal organization, and extracellular matrix mechanics. *Biophys. J.* **2006**, *90* (10), 3762−3773.
(71) Genchi, G. G.; Ciofani, G.; Liakos, I.; Ricotti, L.; Ceseracciu, L.; Athanassiou, A.; Mazzolai, B.; Menciassi, A.; Mattoli, V. Bio/non-bio interfaces: A straightforward method for obtaining long term PDMS/muscle cell biohybrid constructs. *Colloids Surf., B* **2013**, *105*, 144−151.
(72) Peyton, S. R.; Raub, C. B.; Keschrumrus, V. P.; Putnam, A. J. The use of poly(ethylene glycol) hydrogels to investigate the impact of ECM chemistry and mechanics on smooth muscle cells. *Biomaterials* **2006**, *27* (28), 4881−4893.
(73) Goffin, J. M.; Pittet, P.; Csucs, G.; Lussi, J. W.; Meister, J.-J.; Hinz, B. Focal adhesion size controls tension-dependent recruitment of α-smooth muscle actin to stress fibers. *J. Cell Biol.* **2006**, *172* (2), 259−268.
(74) Rape, A. D.; Guo, W.-h.; Wang, Y.-l. The regulation of traction force in relation to cell shape and focal adhesions. *Biomaterials* **2011**, *32* (8), 2043−2051.

DOI: 10.1021/acs.langmuir.7b02935
Langmuir 2018, 34, 1750−1759